# Suppression of ion migration through cross-linked PDMS doping to enhance the operational stability of perovskite solar cells

Jiachen Kang [a,b], Rong Huang [a], Shuxuan Guo [a], Guanghui Han [a], Xue Sun [a], Irfan Ismail [a], Changzeng Ding [a], Fangsen Li [a], Qun Luo [a,*], Yuanjie Li [b,*], Chang-Qi Ma [a,*]

[a] Printable Electronics Research Center, Suzhou Institute of Nano-Tech and Nano-Bionics, Chinese Academy of Sciences, Suzhou 215123, Jiangsu Province, PR China
[b] School of Electronic Science and Engineering, Xi'an JiaoTong University, Xi'an 710049, Shaanxi Province, PR China

## ARTICLE INFO

## ABSTRACT

Although perovskite solar cells have achieved great development in the device performance, the device stability is still a crucial issue hinder the further development. The ion migration is a main reason for the poor stability of the perovskite solar cells. Here, we use a cross-linking material, polydimethylsiloxane (PDMS) to dope the perovskite layer to improve the operational stability. We systematically studied the effect of curing agent content in PDMS on the device performance and stability. The characterization of perovskite film indicates that PDMS primarily doped in the perovskite layer and as well as enriched at the surface of perovskite film. Doping of PDMS promoted the crystallization of perovskite phase, leading to increase of short circuit density ($J_{SC}$) and fill factor (FF) of the solar cells. In addition, PDMS doping improved the operational stability of device due to the suppressing the migration of iodide ions during aging. Moreover, the higher content of curing agents used in PDMS, the better stability of the devices. This work indicates PDMS doping the perovskite layer with a suitable content of curing agent can produce a better operational stability of the perovskite solar cells.

## 1. Introduction

The organic-inorganic halide perovskite materials perform extraordinary photoelectric property, such as long charge diffusion length (Shi et al., 2015, Dong et al., 2015, Chen et al., 2017a,b, Xing et al., 2013), appropriate bandgap for optical absorption (Stoumpos et al., 2013, Yang et al., 2018a,b, Ergen et al., 2017), and large extinction coefficient (Snaith, 2013, Chen et al., 2017a,b). Profiting from these advantages, the halide perovskite has been widely used in the field of photovoltaics and other optoelectronic devices. Recent year, the perovskite solar cells (PSCs) have achieved rapid development and the power conversion efficiencies (PCEs) have been improved from 3.8% to 25.2% in the past decade (Kojima et al., 2009, Lee et al., 2012, Wang et al., 2019, Yang et al., 2018b). Despite the great improvement of performance, the poor stability of PSCs still inhibits the further commercialization (Rong et al., 2018, Kang et al., 2020). The poor stability of PSCs is mainly originate from the degradation of the perovskite crystals in the ambient environmental due to oxygen (Bryant et al., 2016, Yang et al., 2019), humidity (Song et al., 2016, Yang et al., 2015), heat (Conings et al., 2015), UV illumination (Leijtens et al., 2013, Shlenskaya et al., 2018), and

electric fields leaded decomposition, ion migration, interface reaction, and *etc*. Among them, ion migration was a main factor influencing the poor stability of PSCs (Zhou et al., 2020, Xu et al., 2020, Tan et al., 2020).

Ion migration is considered to be a reason for the poor chemical stability of the perovskite materials (Kang et al., 2020, Eames et al., 2015, Guo et al., 2020). In general, the halide ion in perovskite layer will migrate to the top electrode, resulting in the destruction of perovskite crystal structure and metal electrode (Boyd et al., 2018, Calado et al., 2016, Lee et al., 2019, Li et al., 2017a, Yuan and Huang, 2016, Li et al., 2017a,b, Rivkin et al., 2018). Hoke *et al.* (Hoke et al., 2015) reported that MAPb(Br$_X$I$_{1-X}$)$_3$ perovskite undergo reversible phase segregation and form rich of Br$^-$ and I$^-$ perovskite phases under light exposure, which indicated light inducing migration of halide species in perovskite films. Kato *et al.* (Kato et al., 2015) observed that iodine can escape from the perovskite through the Spiro-OMeTAD and react with a silver electrode after aging devices in air or N$_2$. This phenomenon indicated that halide or halogen migration caused by light, heat, moisture, oxygen, or electric field can cause degradation of metal and the perovskite absorber (Boyd et al., 2019). Therefore, how to suppress ion migration is critical for
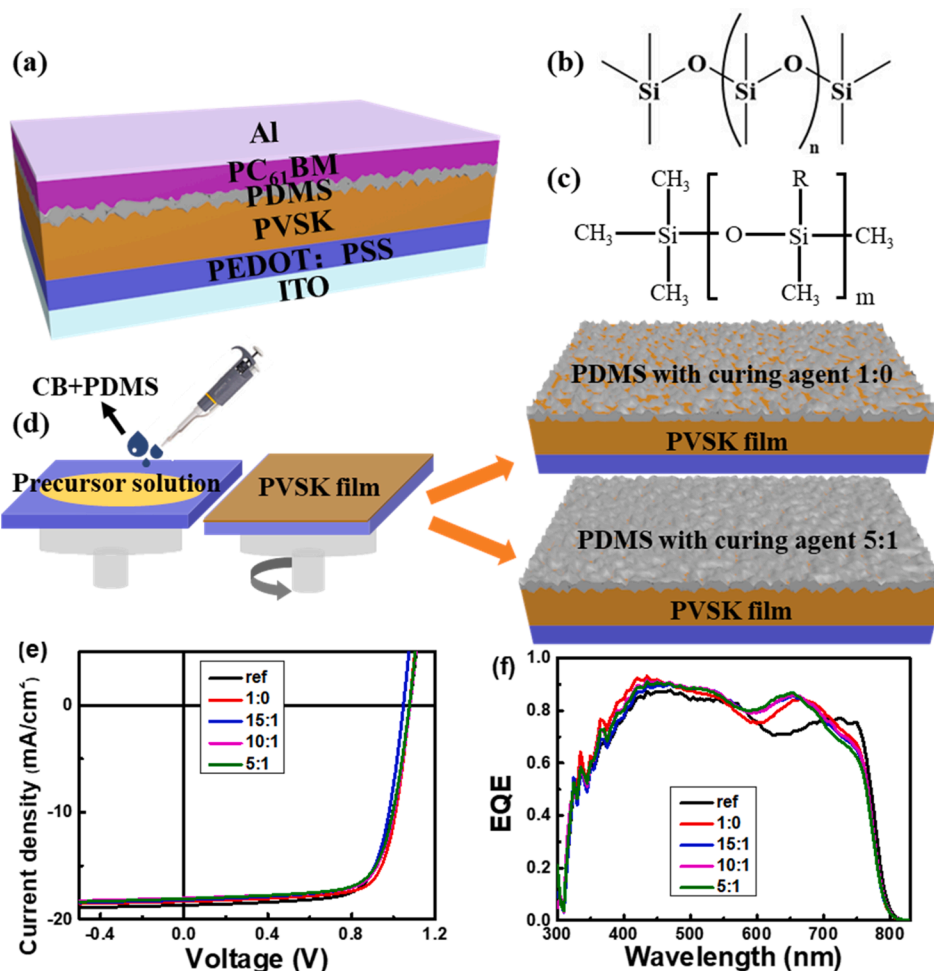
---

**Fig. 1.** (a) The device structure of perovskite solar cells. The molecular structure of (b) PDMS has been cured, and (c) curing agent. (d) The schematic diagram of the film formation process of the doped film without curing agent and with curing agent. (e) *J-V* characteristics and (f) EQE curves of PVSCs with PVSK doped with different PDMS ratios.

improving the stability of PSCs. The previous works showed interface modification and doping of the perovskite layer were effective to solve this problem. Zhou *et al.* (Zhou et al., 2020) introduced a new polar polymer, polycaprolactone (PCL) to passivate the grain boundary (GB) of $MAPbI_3$ perovskite. The devices showed improved stability, remaining 90% of the initial PCE after 400 h storage in ambient, and remained 80% of the efficiency even after 100 h annealing at 85 °C. This effective GB passivation strategy by PCL suggested a great potential of polymer additives toward the stability improvement of PSCs. Li *et al.* (Li et al., 2020a,b) employed an ultrathin 2D nanosheet of oxo-functionalized graphene/dodecylamine (oxo-G/DA) to solve ion migration in cesium (Cs)-formamidine (FA)-methylammonium (MA) triple-cation-based perovskites. The ultrathin 2D network structure could fit tightly on the crystals, wrap and isolate the crystals, and thus reduce the migration of ions within the built-in electric field of the perovskite film. Boyd *et al.* (Boyd et al., 2018) inserted an ITO interface layer underneath the sliver electrode as interface layer by sputtering method to separate the metal electrode from perovskite layer. Using this method, the migration of I and Ag ion was effectively suppressed, and demonstrated improved thermal stability at 85 °C.

Among these various interface passivation and perovskite doping materials, it is conformed that cross-linked materials are potential to promote the stability of perovskite since it can prevent the permeation of oxygen and moisture. For example, Huang *et al.* (Huang et al., 2019) introduced a novel glued poly (ethylene-co-vinyl acetate) (EVA) interfacial layer between the perovskite layer and $PC_{61}BM$, which could

balance charge transfer, inhibit ionic migration, and significantly improve the water resistance of PSCs. Li *et al.* (Li et al., 2020a,b) introduced a novel crosslinked PCBM (CL-PCBM) interlayer at the perovskite/electron transport layer (ETL) interface. The CL-PCBM interlayer was prepared by UV cross-linking technique, which improved the quality of the resultant perovskite film and the charge transfer capability of the ETL. The PSC devices integrating the CL-PCBM interlayers exhibited superior humidity and UV stabilities. Kim *et al.* (Kim et al., 2019) demonstrated that polydimethylsiloxane (PDMS) could passivate the adjacent grain boundaries (GBs) of the perovskite crystals. The device can maintain more than 90% of the initial PCE (15%) after laboratory storage for 5000 h under 70% relative humidity. Although these works proved doping PDMS could improve the humidity stability of device, the effect of PDMS doping on the ion migration is still not clear. In addition, PDMS usually form cross-linked films through adding curing agents. Therefore, the content of curing agent would highly impact the crosslink degree. So, it is necessary to optimize the content of curing agent in PDMS to further improve the operational stability of the device.

In this work, we systematically studied the effect of PDMS concentration and curing agent content on the device performance and stability of PSCs. The result demonstrated doping a suitable concentration of PDMS solution could improve the stability of PSCs without impacting the device performance. Furthermore, the content of curing agent in PDMS influenced the device stability as well. The higher curing agent content enabled better stability of PSCs. The Time of Flight Second Ion

**Table 1**
The device performance with PDMS doped perovskite film as the active layer.

| Ratio of PDMS to curing agent | $V_{OC}$ (V) | $J_{SC}$ (mA cm$^{-2}$) | FF | PCE$_{ave}$ (%) | PCE$_{max}$ (%) | $R_S$ ($\Omega$ cm$^2$) | $R_{SH}$ ($\Omega$ cm$^2$) |
|---|---|---|---|---|---|---|---|
| ref | 1.07 ± 0.01 | 20.06 ± 0.17 | 0.71 ± 0.01 | 15.24 ± 0.16 | 15.40 | 7.31 | 1387.06 |
| 1:0 | 1.06 ± 0.02 | 20.59 ± 0.47 | 0.73 ± 0.01 | 15.93 ± 0.57 | 16.50 | 6.65 | 1489.18 |
| 15:1 | 1.05 ± 0.01 | 20.57 ± 0.41 | 0.73 ± 0.01 | 15.77 ± 0.37 | 16.14 | 6.73 | 1555.49 |
| 10:1 | 1.06 ± 0.02 | 20.77 ± 0.34 | 0.73 ± 0.01 | 16.07 ± 0.23 | 16.30 | 7.00 | 1888.60 |
| 5:1 | 1.06 ± 0.01 | 20.58 ± 0.60 | 0.73 ± 0.01 | 15.92 ± 0.41 | 16.33 | 7.01 | 1588.53 |
| 2:1 | 1.05 ± 0.02 | 15.63 ± 0.78 | 0.68 ± 0.2 | 11.18 ± 0.56 | 11.64 | 7.94 | 1503.26 |
| 1:1 | 0.98 ± 0.04 | 15.12 ± 0.85 | 0.59 ± 0.3 | 8.42 ± 0.38 | 8.80 | 8.42 | 942.08 |

Mass Spectrometry (ToF-SIMS) result revealed that cross-linked PDMS could prevent the migration process of iodine ions to top electrode and suppress the formation of PbI$_2$ during the aging period. The characterization of perovskite film illustrated PDMS mainly selectively enriched on the surface of PVSK film. The steady-state fluorescence spectrum proved that the introduction of PDMS could promote the charge transfer efficiency at the PVSK/PCBM interface. This work provides a simple strategy to inhibit the migration of I ions and improve the device stability through doping the perovskite layer with a cheap and commonly used cross-link agent PDMS.

## 2. Experiment sections

PEDOT: PSS (Al 4083) was purchased from Heraeus Ltd. Lead chloride (PbCl$_2$, 99%), Lead iodide (PbI$_2$, 99%), Methylammonium Iodide (MAI, 99.5%) were purchased from Xi'an Polymer Light Technology Corp. (6,6)-phenyl-C$_{61}$-butyric acid methyl ester (PC$_{61}$BM) was bought from Sigma-Aldrich. PDMS was purchase from Dow Corning Sylgard 184. PDMS and the curing agent were mixed together with different volume ratios, then chlorobenzene (CB) was added and stirred to form the diluted solution.

The detailed fabrications process was described as follow: PEDOT: PSS (4083) hole transport layer was spin-coated on top of glass/ITO substrate at 3500 rpm for 45 s. Then, the film was annealed at 130 °C for 10 min and transferred into the N$_2$-filled glove box to deposit the perovskite film and PC$_{61}$BM layers. Before that, the perovskite precursor solution was prepared by dissolving 103.3 mg of methylamine iodide (MAI), 310.10 mg of lead iodide (PbI$_2$) and 9.72 mg of lead chloride (PbCl$_2$) in the mixture of C$_4$H$_6$O$_2$ (GBL) C$_2$H$_6$OS (DMSO) (7:3 v/v) at 50–60 °C and stirred for at least 2 h. The perovskite films were deposited by a consecutive two-step spin-coating process at 1000 rpm for 10 s, and at 4000 rpm for 30 s. During the second-step spin-coating at 17 s, 400 µL antisolvent anhydrous chlorobenzene was dropped onto the center of the film. The PDMS doped PVSK films were fabricated with the same route as the pristine film by using the CB solution containing PDMS as the antisolvent. After that the perovskite layer was annealed at 100 °C for 10 min. After cooling to room temperature, the PC$_{61}$BM solution (20 mg/mL in chlorobenzene) was spin-coated onto the perovskite film at 1000 rpm for 45 s. Finally, 100 nm-thick Al was deposited on the PC$_{61}$BM film through a shadow mask under a vacuum of 10$^{-5}$ torr.

The absorption spectra were measured by the Lamada 750 UV–vis–NIR Spectro-photometer (PerkinElmer). The micrograph was investigated by Scanning Electron Microscope (SEM, S-4800). Steady-state and transient-state photoluminescence were tested using the fluorescence spectrometer (JY Fluorolog-3-Tou). The Time-of-Flight Secondary Ion Mass Spectrometry (ToF-SIMS) was recorded by TOF-SIMS 5–100. The J–V characteristics of devices were measured in glove box using a Keithley model 2400 source measurement unit. The EQE was measured using a home-made IPCE system consisting of a 150 W tungsten halogen lamp (Osram 64642), a monochromator (Zolix, Omni-l300), an optical chopper, and an I–V converter (QE-IV Convertor, Suzhou D&R Instruments) equipped with lock-in amplifier (Stanford Research Systems SR 830). To better simulate the device under one sun condition, bias light from a 532 nm solid-state laser was introduced to the cell simultaneously. A calibrated Si solar cell was used as a reference. The unencapsulated cells was tested in a sealed box.
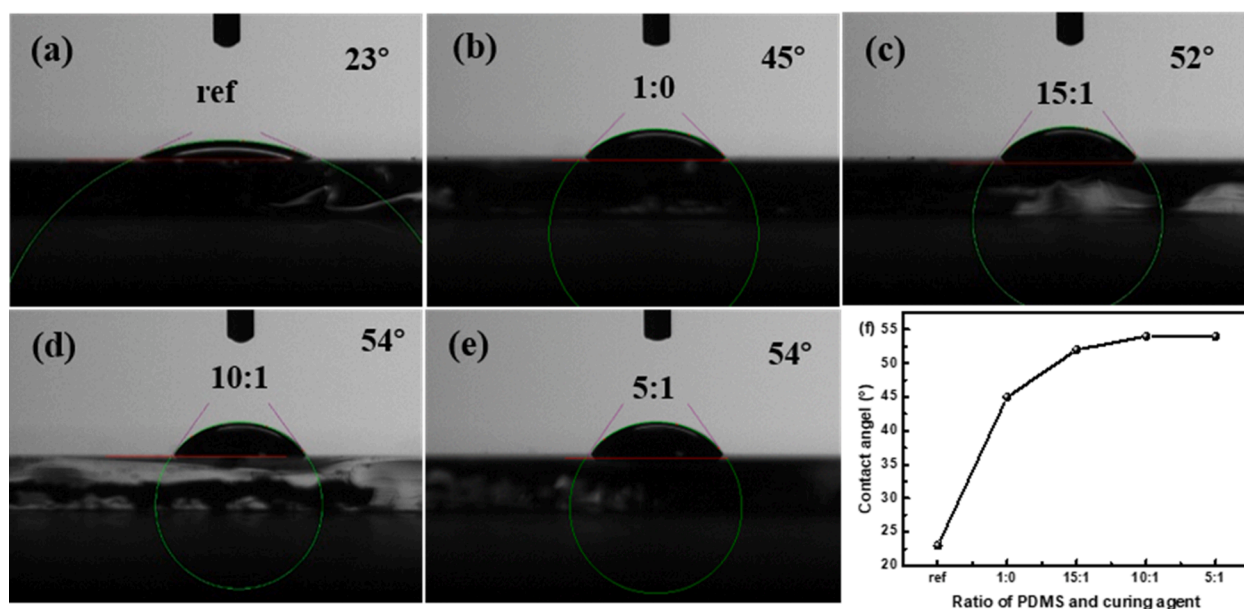


**Fig. 2.** The contact angel between the PVSK films with diiodomethane, (a) PVSK film, PDMS doped PVSK films with ratios of PDMS to curing agent as (b) 1:0, (c) 15:1, (d) 10:1, and (e) 5:1. (f) The variation trend between contact angel and PDMS.
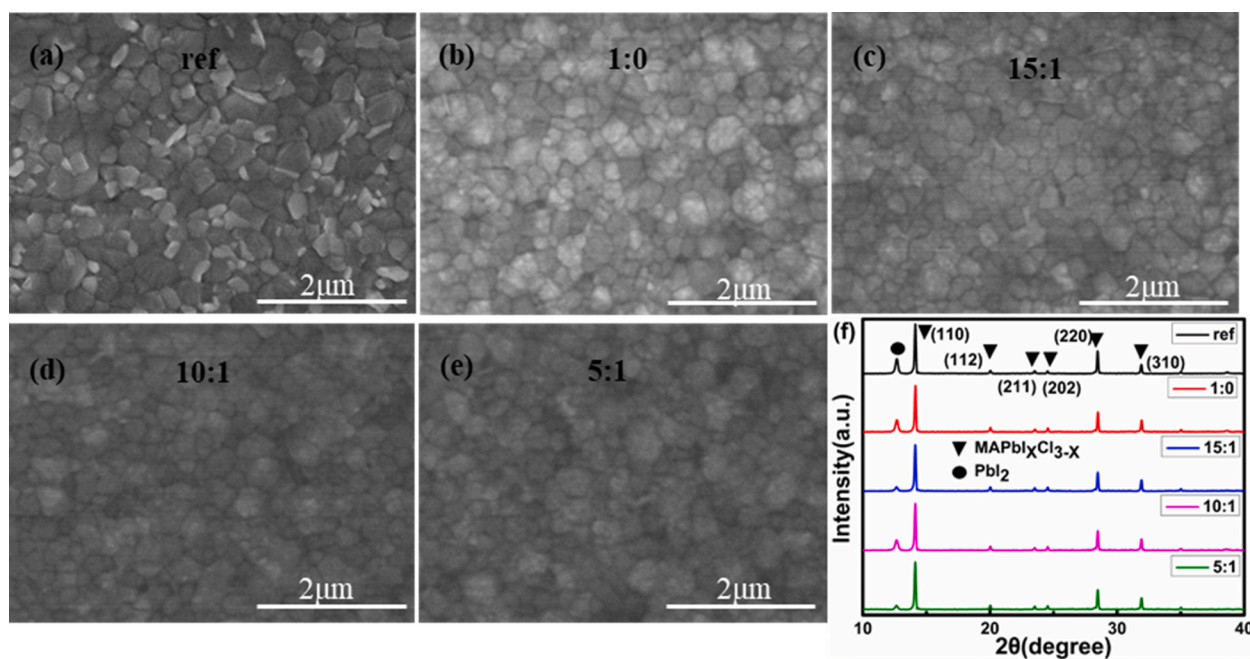
**Fig. 3.** The scanning electron microscope (SEM) images of the PVSK films, (a) PVSK film, PVSK films doped PDMS with ratio of PMDS to curing agent as (b) 1:0, (c) 15:1, (d) 10:1, and (e) 5:1. (f) The X-ray diffraction (XRD) patterns of the PVSK films doped with PDMS with different curing agent contents.

## 3. Results and discussion

Fig. 1(a) shows the device structure of the perovskite solar cells and Fig. 1(b) and (c) show the molecular structure of the cross-linked PDMS and curing agent. Fig. 1(d) depicts the film formation process of PDMS doped PVSK films. The schematic diagram of doped films with curing agent and w/o curing agent was illustrated in Fig. 1(d) as well. PDMS could form a denser cross-linked structure after introducing curing agent. Different PDMS curing agent contents led to different PDMS curing behaviors. Thus, we systematically tested the impact of curing agent content to the device performance and stability. The *J-V* characteristics and external quantum efficiency (EQE) curves of the devices with PDMS doped PVSK layers are presented in Fig. 1(e–f), and Table 1 lists the device performance parameters. The reference sample is the device doped neither with PDMS nor curing agent. The reference device gave a short circuit current density ($J_{SC}$) of $20.06 \pm 0.31$ mA cm$^{-2}$, an open-circuit voltage ($V_{OC}$) of $1.07 \pm 0.01$ V, a fill factor (FF) of $0.71 \pm 0.01$. And a best power conversion efficiency (PCE) of 15.40% and an average PCE of 15.24% were obtained from reverse scan. With PDMS doped PVSK films, the devices showed slight improved performance. The champion PCE reached up to 16.30% when the ratio of curing agent was 10:1. The improvement of $J_{SC}$ and FF for the PDMS

doped PSCs could be ascribed to the reduce of charge recombination due to the reduced crystals defects. As shown in Table 1, further increasing the concentration of the curing agent to 2:1 and 1:1, the device performance rapidly decreased to 11.64% and 8.80%. The decrease of the device performance might be ascribed to the decline of perovskite crystal quality.

In order to further figure out the impact of PMDS doping to the crystallization and morphology of the PVSK films. The surface energy, XRD patterns, and the SEM images of the films were studied. The contact angle of a drop of diiodomethane on top of these PVSK films was measured and showed in Fig. 2. It showed a distinct difference in the contact angle between the doped films and diiodomethane in comparison with that the pristine films. As shown in Fig. 2(a), the reference film without PDMS showed a contact angle of 23°. With PDMS doping, the contact angle significantly increased to be about 50°. And with the increase of curing agent content, the contact angle increased gradually from 45° to 54°. A largest contact angle of 54° was observed with doping PDMS ratio of 10:1 and 5:1. We know polydimethylsiloxane (PDMS) is a typical low surface-energy material, which would decrease the surface energy of the films (Ye et al., 2018). However, the perovskite films would be corroded by water and decompose to $PbI_2$ and MAI though PDMS was covered on the top of the perovskite films in the work. So, it is
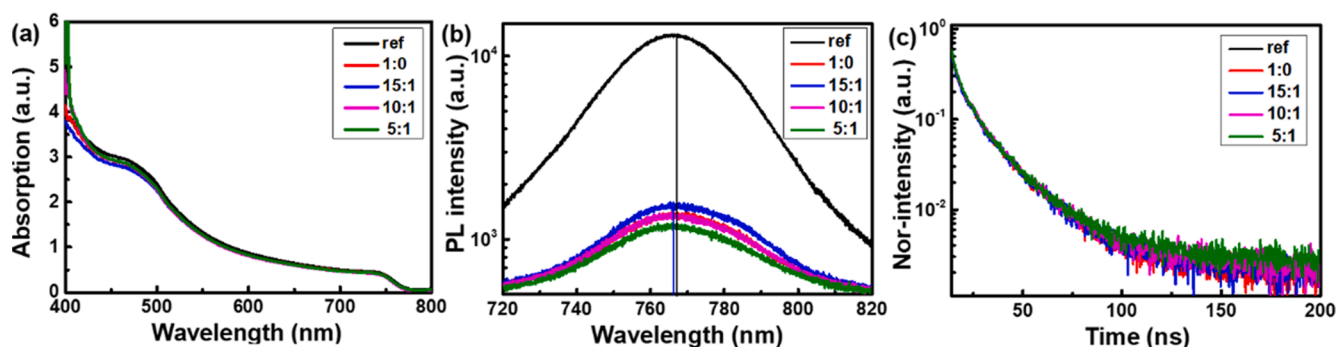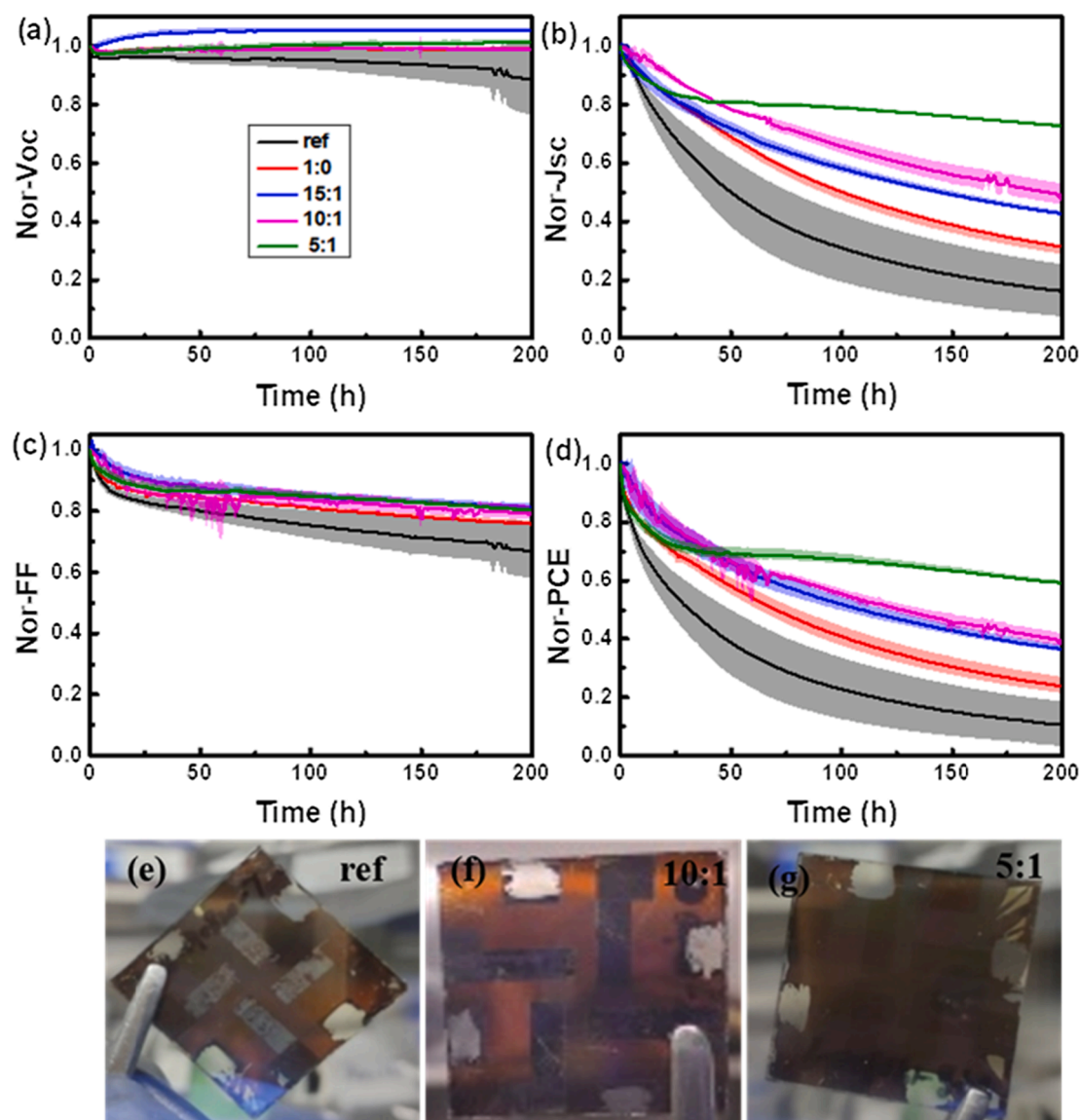


**Fig. 4.** The optical characterization of doping perovskite film, (a) UV–vis absorption spectra, (b) steady-state PL spectra, and (c) time-resolved PL spectra of the $PC_{61}BM$/perovskite films.

**Fig. 5.** (a-d) The evolution of the device performance of the perovskite solar cells doped with PDMS. The photographs of the aged devices seen from back side, (e) reference device without PDMS and curing agent; (f) PDMS doped device with PDMS and curing agent ratio of 10:1, (g) PDMS doped device with ratio of PDMS to curing agent of 5:1.

difficult to test the contact angle of water on the top of the MAPbI₃ perovskite films. Thus, only the contact angle between the PVSK films with diiodomethane was tested herein, and the surface energy can't be calculated only with these data. Nevertheless, the gradual increase of contact angle (Fig. 2(f)) between the perovskite films with diiodo-methane indicated the films became more hydrophobic. Since PDMS is typically hydrophobic, the increased contact angle suggested the successful doping of PDMS in the PVSK films.

Fig. 3(a–e) show the top-view scanning electron microscope (SEM) images of the PVSK films. In Fig. 3(a), we found the reference film have darker grain and brighter grain, which could be ascribed to the perovskite and PbI₂ phase, respectively. The grain size of the PVSK phase is approximately 300 nm, and the lead iodide phase has a grain size of about 200 nm and a width of about 100 nm. For the PDMS-doped PVSK films (Fig. 3(b–e)), the amount the bright PbI₂ phase was greatly decrease. But PDMS doping did not cause the change of crystals size of PVSK. The X-ray diffraction (XRD) patterns of the PVSK films were tested to further investigate the change of crystallization, and results were showed in Fig. 3(f). The XRDs patterns showed these PVSK films contained typical diffraction peaks at 12.7°, 14.1°, 28.4° and 31.8°. The

typical diffraction peaks at 12.7°and 14.1°corresponded to the typical phase of PbI₂ and PVSK, respectively. Compared to the pristine PVSK films without PDMS doping, the films with PDMS doping showed weaker diffraction peaks of PbI₂, indicating crystallization process of PbI₂ are suppressed. As previously reported, the formation of PVSK crystals was formed by the reaction of PbI₂ and MAI in precursor solution. Thus, it is reasonable to speculate that doping PDMS in the PVSK films could facilitate transformation from the precursor to perovskite crystals. (Mabrouk et al., 2017)

Then, the optical properties of the perovskite film after adding PDMS was investigated. From the UV–Vis absorption spectra in Fig. 4(a), no significant distinction was observed. The similar absorption spectra illustrated that PDMS doping did not impact the thickness of perovskite film. We also tested the photoluminescence (PL) spectra of the PC₆₁BM/PVSK film, as showing in Fig. 4(b–c). Steady state fluorescence spectrum showed the PDMS doped films presented much weaker PL intensity relative to the pristine films. Specifically, the PL intensity reduced to be about one third of the reference film. This result revealed improved charge transfer between PC₆₁BM and PVSK as the perovskite films were doped with PDMS. The transient PL spectra of the films (Fig. 4(c))
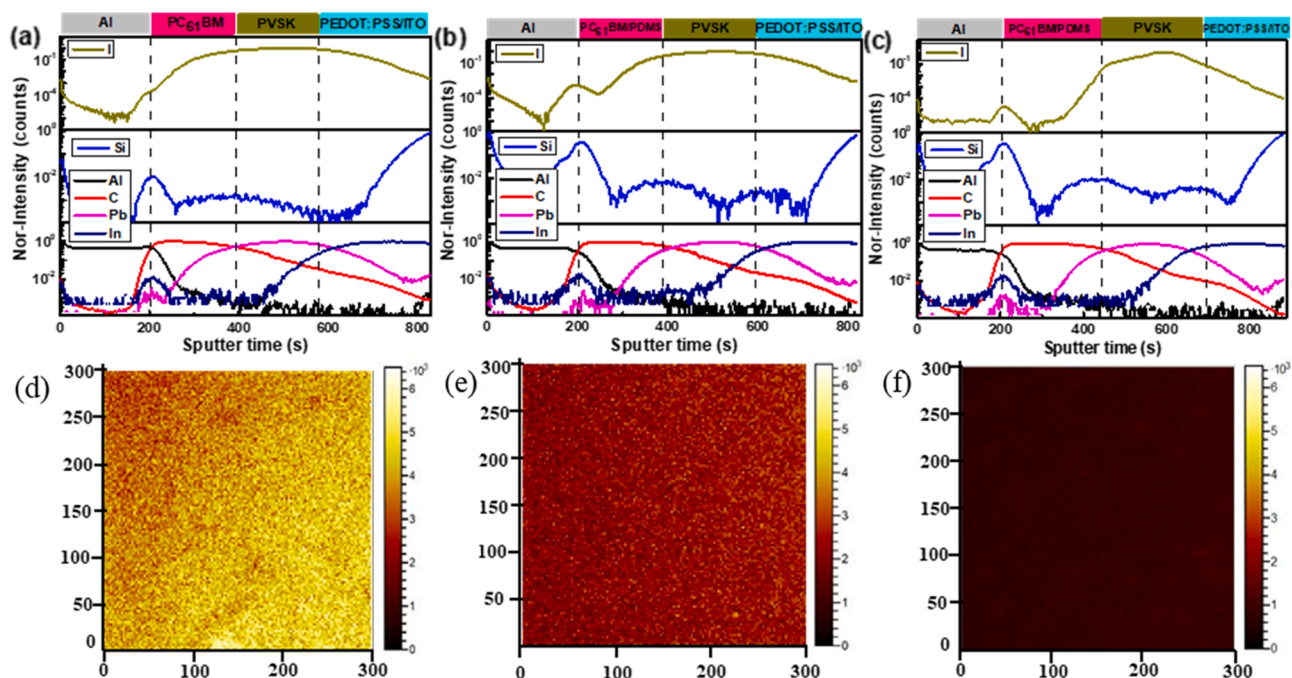
**Fig. 6.** The second ion mass spectroscopy (SIMS) result with aging device, (a) reference device, (b),(c) doped device with PDMS ratio of 10:1 and 5:1 respectively. The distribution of I element in the aged devices, (d) reference device, (b) (c) doped devices with PDMS ratio of 10:1 and 5:1, respectively.

showed a similar decay curve. According to the transient PL spectra, we can calculate the average carrier lifetime of the perovskite films through curves fitting with double exponential decay function. The PVSK films without PDMS and with PDMS exhibited a similar lifetime of 8–9 ns. Time-resolved photoluminescence spectra didn't show an obvious distinction of fluorescence lifetime.

The operational stability of the devices with different curing agent contents were tested under continuous illumination in the glove box, and the evolution of the performance parameters are presented in Fig. 5. As shown in Fig. 5(a), there were no significant decay of $V_{OC}$ during aging time for all the devices. But the $J_{SC}$ and FF (Fig. 5(b)–(c)) showed continuous degradation during 200 h's illumination, which lead to the performance decay of PCE (Fig. 5(d)). PDMS doping have slowed down the decay speed, especially for the degradation of $J_{SC}$. The reference device only maintained about 20% of the initial value after 200 h. The doped devices could maintain 40–60% of the initial $J_{SC}$. Moreover, it is apparent that the higher PDMS curing agent will decrease the decay of better $J_{SC}$. As an optimization, the device with ratio of curing agent (ratio of PDMS to curing agent of 5:1) maintained about 72% of the initial value. The PCE decay trends were similar to the $J_{SC}$. The pictures of the aged devices were showed as Fig. 5(e–f). We can see the aged Al electrode from view of ITO sides, which is because of chemical reaction between Al electrode and I ions due to I migration. And a similar phenomenon was observed in the PDMS doped device without curing agent (ratio of 1:0). In contrast, the PDMS doped device with curing agent ratio of 5:1 did not show the similar phenomenon. The sample w/o curing agent would not from cross-linked networks. The difference between the sample with curing agent and w/o curing agent is whether PDMS was cross-linked or not. So, we can conclude that the non-cross-linked doping could only slightly improve the durability of device during long-term illumination, whereas cross-linked doping was much more effective. This result indicated it is necessary to suppress ion migration through cross-linking doping.

In order to further figure out the degradation mechanism of the PSCs. We use ToF-SIMS to analyze the distribution of elements in the aged devices. Fig. 6(a–c) show the ToF-SIMS images of the aged devices of the PVSK w/o and with PDMS doping (with ratio of PDMS to curing agent of of 5:1). By analyzing the changes of Al, C, Si, Pb elements, the corresponding interfaces of Al, PC$_{61}$BM/PDMS, PVSK and ITO layers were determined. Similar results were observed in the devices w/o PDMS and with PDMS ratio of 5:1, indicated the introduction of PDMS did not cause obvious change of elemental distribution among the devices. However, the ToF-SIMS result showed a big difference in I ion between these aged devices. For the pristine PVSK without PDMS doping, obvious signals of I ions could be seen in the PC$_{61}$BM layer. It is evident to see that I ions have migrated into the PC$_{61}$BM layer from perovskite layer. In the case of PDMS doping without curing agent, the intensity of I ions was lower than that in the pristine PSC. However, the signals of I ions was still obvious, suggesting the ion migration from the PVSK to PC$_{61}$BM films was partly suppressed. Whereas, there is no signals of I ions for the crosslinked PDMS doped PSCs (Fig. 6(c)). The phenomenon clearly showed the doping of cross-linked PDMS in the PVSK films could effectively prevent the ion migration. In addition, we can clearly see the enhancement of Si signal in the PDMS doped films and the interface of PVSK(PCBM)/Al. The result indicated PDMS might enrich on the surface of PVSK(PCBM) film and within the perovskite films in the grain boundaries, which have inhibited the migration of I ion. We also detected the change of surface elements from top electrode view by SIMS mapping result. The SIMS mapping also showed a significant change of I ion between the aged devices in Fig. 6(d–f). The aggregation of I element on the surface of top electrode was observed in the reference device. The migration of I ion into the electrode layer is the main reason for the poor working stability of the reference device. The sample with un-crosslinked PDMS also showed the aggregation of I, which indicated that the un-crosslinked PDMS could not prevent the migration of I ions. However, nearly no signal of I could be observed for the sample with crosslinked PDMS (with ratio of curing agent of 5:1). Thus, the better stability of the crosslinked PDMS doped device may cause by the compact crosslinked PDMS interfacial layer after adding curing agent. With a higher ratio of curing agent, the degree of cross-linking increased, and PDMS would become more compact. Therefore, a better operational stability was achieved with the increase of PDMS to curing agent ratio from 15:1 to 5:1. But as the ratio exceeds 5:1, the device performance decreased. Therefore, we can confirm that 5:1 is a suitable ratio of PDMS to curing agent to promote stability without reduce performance of device.
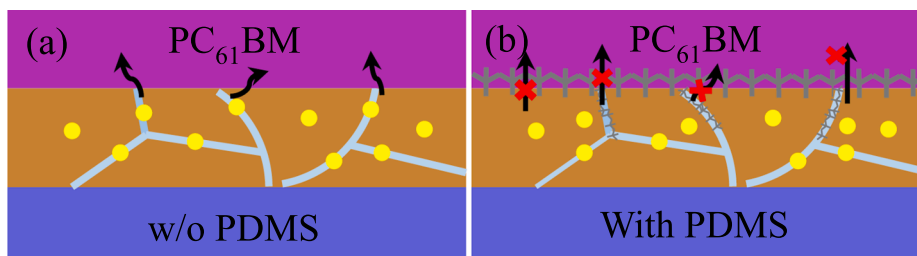
**Fig. 7.** The schematic diagram of doped PDMS to inhibit migration of I ion, (a) w/o PDMS, (b) with cross-linked PDMS.

According to the ToF-SIMS results, it is reasonable to speculate that PDMS not only doped in the PVSK layer, which might appear in the crystal boundaries, but also enriched on top of the PVSK(PCBM) films. Both the formation of a surface suppression layer and crystal boundaries bonding reduced ion migration. Thus, the schematic diagram of the doped PVSK films was showed in Fig. 7. The black arrows stood for ion migration in the perovskite films. The blue lines stood for the grain boundaries.

## 4. Conclusions

In this work, we use polydimethylsiloxane (PDMS), a cross-linking material, as the dopant and barrier layer to promote the device stability. We systematically optimized the content of curing agent in PDMS. The results indicated that PDMS was not only inside in PVSK film, but also enriched on the surface of perovskite layer to form an interface layer, which effectively suppressed the migration of I ion to the upper layer. The PDMS doping could reduce the $PbI_2$ residual phase and promote the crystallization transition of PVSK. The PDMS doped cell presented a slight improvement of performance compared to the pristine devices. The working stability was significantly improved due to the suppression of migration process. In this work, we testify an effective cross-linked strategy to improve the stability of perovskite solar cells.

## Declaration of Competing Interest

The authors declare that they have no known competing financial interests or personal relationships that could have appeared to influence the work reported in this paper.

## Acknowledgements

## References

Shi, D., Adinolfi, V., Comin, R., Yuan, M., Alarousu, E., Buin, A., Chen, Y., Hoogland, S., Rothenberger, A., Katsiev, K., Losovyj, Y., Zhang, X., Dowben, P.A., Mohammed, O. F., Sargent, E.H., Bakr, O.M., 2015. Low trap-state density and long carrier diffusion in organolead trihalide perovskite single crystals. Science 347 (6221), 519–522. https://doi.org/10.1126/science.aaa2725.

Dong, Q., Fang, Y., Shao, Y., Mulligan, P., Qiu, J., Cao, L., Huang, J., 2015. Electron-hole diffusion lengths > 175 μm in solution-grown $CH_3NH_3PbI_3$ single crystals. Science 347 (6225), 967–970. https://doi.org/10.1126/science.aaa5760.

Chen, H., Ye, F., Tang, W., He, J., Yin, M., Wang, Y., Xie, F., Bi, E., Yang, X., Grätzel, M., Han, L., 2017a. A solvent- and vacuum-free route to large-area perovskite films for efficient solar modules. Nature 550 (7674), 92–95. https://doi.org/10.1038/nature23877.

Xing, G., Mathews, N., Sun, S., Lim, S.S., Lam, Y.M., Grätzel, M., Mhaisalkar, S., Sum, T. C., 2013. Long-range balanced electron- and hole-transport lengths in organic-inorganic $CH_3NH_3PbI_3$. Science 342 (6156), 344–347. https://doi.org/10.1126/science.1243167.

Stoumpos, C.C., Malliakas, C.D., Kanatzidis, M.G., 2013. Semiconducting tin and lead iodide perovskites with organic cations: phase transitions, high mobilities, and near-infrared photoluminescent properties. Inorg. Chem. 52 (15), 9019–9038. https://doi.org/10.1021/ic401215x.

Yang, T.-C.-J., Fiala, P., Jeangros, Q., Ballif, C., 2018a. High-bandgap perovskite materials for multijunction solar cells. Joule 2 (8), 1421–1436. https://doi.org/10.1016/j.joule.2018.05.008.

Ergen, O., Gilbert, S.M., Pham, T., Turner, S.J., Tan, M.T.Z., Worsley, M.A., Zettl, A., 2017. Graded bandgap perovskite solar cells. Nat. Mater. 16 (5), 522–525. https://doi.org/10.1038/nmat4795.

Snaith, H.J., 2013. Perovskites: The emergence of a new era for low-cost, high-efficiency solar cells. J. Phys. Chem. Lett. 4 (21), 3623–3630. https://doi.org/10.1021/jz4020162.

Chen, Z., Dong, Q., Liu, Y., Bao, C., Fang, Y., Lin, Y., Tang, S., Wang, Q., Xiao, X., Bai, Y., Deng, Y., Huang, J., 2017b. Thin single crystal perovskite solar cells to harvest below-bandgap light absorption. Nat. Commun. 8 (1), 1890. https://doi.org/10.1038/s41467-017-02039-5.

Kojima, A., Teshima, K., Shirai, Y., Miyasaka, T., 2009. Organometal halide perovskites as visible-light sensitizers for photovoltaic cells. J. Am. Chem. Soc. 131 (17), 6050–6051. https://doi.org/10.1021/ja809598r.

Lee, M.M., Teuscher, J., Miyasaka, T., Murakami, T.N., Snaith, H.J., 2012. Efficient hybrid solar cells based on meso-superstructured organometal halide perovskites. Science 338 (6107), 643–647. https://doi.org/10.1126/science.1228604.

Wang, L., Zhou, H., Hu, J., Huang, B., Sun, M., Dong, B., Zheng, G., Huang, Y., Chen, Y., Li, L., Xu, Z., Li, N., Liu, Z., Chen, Q., Sun, L.-D., Yan, C.-H., 2019. A $Eu^{3+}$-$Eu^{2+}$ ion redox shuttle imparts operational durability to Pb-I perovskite solar cells. Science 363 (6424), 265–270. https://doi.org/10.1126/science.aau5701.

Yang, D., Yang, R., Wang, K., Wu, C., Zhu, X., Feng, J., Ren, X., Fang, G., Priya, S., Liu, S. F., 2018b. High efficiency planar-type perovskite solar cells with negligible hysteresis using EDTA-complexed $SnO_2$. Nat. Commun. 9 (1), 3239. https://doi.org/10.1038/s41467-018-05760-x.

Rong, Y., Hu, Y., Mei, A., Tan, H., Saidaminov, M.I., Seok, S.I., McGehee, M.D., Sargent, E.H., Han, H., 2018. Challenges for commercializing perovskite solar cells. Science 361 (6408), eaat8235. https://doi.org/10.1126/science.aat8235.

Kang, J., Han, K., Sun, X., Zhang, L., Huang, R., Ismail, I., Wang, Z., Ding, C., Zha, W., Li, F., Luo, Q., Li, Y., Lin, J., Ma, C.-Q., 2020. Suppression of Ag migration by low-temperature sol-gel zinc oxide in the Ag nanowires transparent electrode-based flexible perovskite solar cells. Org. Electron. 82 (2020), 105714 https://doi.org/10.1016/j.orgel.2020.105714.

Bryant, D., Aristidou, N., Pont, S., Sanchez-Molina, I., Chotchunangatchaval, T., Wheeler, S., Durrant, J.R., Haque, S.A., 2016. Light and oxygen induced degradation limits the operational stability of methylammonium lead triiodide perovskite solar cells. Energy Environ. Sci. 9 (5), 1655–1660. https://doi.org/10.1039/C6EE00409A.

Yang, T.-Y., Jeon, N.J., Shin, H.-W., Shin, S.S., Kim, Y.Y., Seo, J., 2019. Achieving long-term operational stability of perovskite solar cells with a stabilized efficiency exceeding 20% after 1000 h. Adv. Sci. 6 (14), 1900528. https://doi.org/10.1002/advs.201900528.

Song, Z., Abate, A., Watthage, S.C., Liyanage, G.K., Phillips, A.B., Steiner, U., Graetzel, M., Heben, M.J., 2016. Perovskite solar cell stability in humid air: partially reversible phase transitions in the $PbI_2$-$CH_3NH_3I$-$H_2O$ system. Adv. Energy Mater. 6 (19), 1600846. https://doi.org/10.1002/aenm.201600846.

Yang, J., Siempelkamp, B.D., Liu, D., Kelly, T.L., 2015. Investigation of $CH_3NH_3PbI_3$ degradation rates and mechanisms in controlled humidity environments using in situ techniques. ACS Nano 9 (2), 1955–1963. https://doi.org/10.1021/nn506864k.

Conings, B., Drijkoningen, J., Gauquelin, N., Babayigit, A., D'Haen, J., D'Olieslaeger, L., Ethirajan, A., Verbeeck, J., Manca, J., Mosconi, E., Angelis, F.D., Boyen, H.-G., 2015. Intrinsic thermal instability of methylammonium lead trihalide perovskite. Adv. Energy Mater. 5 (15), 1500477. https://doi.org/10.1002/aenm.201500477.

Leijtens, T., Eperon, G.E., Pathak, S., Abate, A., Lee, M.M., Snaith, H.J., 2013. Overcoming ultraviolet light instability of sensitized $TiO_2$ with meso-superstructured organometal tri-halide perovskite solar cells. Nat. Commun. 4 (1), 2885. https://doi.org/10.1038/ncomms3885.

Shlenskaya, N.N., Belich, N.A., Grätzel, M., Goodilin, E.A., Tarasov, A.B., 2018. Light-induced reactivity of gold and hybrid perovskite as a new possible degradation mechanism in perovskite solar cells. J. Mater. Chem. A 6 (4), 1780–1786. https://doi.org/10.1039/C7TA10217H.

Zhou, Y., Yin, Y., Zuo, X., Wang, L., Li, T.-D., Zhou, Y., Padture, N.P., Yang, Z., Guo, Y., Xue, Y., Kisslinger, K., Cotlet, M., Nam, C.-Y., Rafailovich, M.H., 2020. Enhancing chemical stability and suppressing ion migration in $CH_3NH_3PbI_3$ perovskite solar cells via direct backbone attachment of polyesters on grain boundaries. Chem. Mater. 32 (12), 5104–5117. https://doi.org/10.1021/acs.chemmater.0c00995.

Xu, Z., Wang, L., Han, Q., Kamata, Y., Ma, T., 2020. Suppression of iodide ion migration via Sb₂S₃ interfacial modification for stable inorganic perovskite solar cells. ACS Appl. Mater. Interf. 12 (11), 12867–12873. https://doi.org/10.1021/acsami.9b23630.

Tan, S., Yavuz, I., De Marco, N., Huang, T., Lee, S.-J., Choi, C.S., Wang, M., Nuryyeva, S., Wang, R., Zhao, Y., Wang, H.-C., Han, T.-H., Dunn, B., Huang, Y., Lee, J.-W., Yang, Y., 2020. Steric impediment of ion migration contributes to improved operational stability of perovskite solar cells. Adv. Mater. 32 (11), 1906995. https://doi.org/10.1002/adma.201906995.

Eames, C., Frost, J.M., Barnes, P.R.F., O'Regan, B.C., Walsh, A., Islam, M.S., 2015. Ionic transport in hybrid lead iodide perovskite solar cells. Nat. Commun. 6 (1), 7497. https://doi.org/10.1038/ncomms8497.

Guo, S., Sun, X., Ding, C., Huang, R., Tan, M., Zhang, L., Luo, Q., Li, F., Jin, J., Ma, C.-Q., 2020. Non-uniform chemical corrosion of metal electrode of p–i–n type of perovskite solar cells caused by the diffusion of CH₃NH₃I. Energy Technol. 8 (12), 2000250. https://doi.org/10.1002/ente.202000250.

Boyd, C.C., Cheacharoen, R., Bush, K.A., Prasanna, R., Leijtens, T., McGehee, M.D., 2018. Barrier design to prevent metal-induced degradation and improve thermal stability in perovskite solar cells. ACS Energy Lett. 3 (7), 1772–1778. https://doi.org/10.1021/acsenergylett.8b00926.

Calado, P., Telford, A.M., Bryant, D., Li, X., Nelson, J., O'Regan, B.C., Barnes, P.R.F., 2016. Evidence for ion migration in hybrid perovskite solar cells with minimal hysteresis. Nat. Commun. 7 (1), 13831. https://doi.org/10.1038/ncomms13831.

Lee, J.-W., Kim, S.-G., Yang, J.-M., Yang, Y., Park, N.-G., 2019. Verification and mitigation of ion migration in perovskite solar cells. APL Mater. 7 (4), 041111 https://doi.org/10.1063/1.5085643.

Li, C., Guerrero, A., Zhong, Y., Gräser, A., Luna, C.A.M., Köhler, J., Bisquert, J., Hildner, R., Huettner, S., 2017a. Real-time observation of iodide ion migration in methylammonium lead halide perovskites. Small 13 (42), 1701711. https://doi.org/10.1002/smll.201701711.

Yuan, Y., Huang, J., 2016. Ion migration in organometal trihalide perovskite and its impact on photovoltaic efficiency and stability.ACC. Chem. Res. 49 (2), 286–293. https://doi.org/10.1021/acs.accounts.5b00420.

Li, Z., Xiao, C., Yang, Y., Harvey, S.P., Kim, D.H., Christians, J.A., Yang, M., Schulz, P., Nanayakkara, S.U., Jiang, C.-S., Luther, J.M., Berry, J.J., Beard, M.C., Al-Jassim, M. M., Zhu, K., 2017b. Extrinsic ion migration in perovskite solar cells. Energy Environ. Sci. 10 (5), 1234–1242. https://doi.org/10.1039/C7EE00358G.

Rivkin, B., Fassl, P., Sun, Q., Taylor, A.D., Chen, Z., Vaynzof, Y., 2018. Effect of ion migration-induced electrode degradation on the operational stability of perovskite solar cells. ACS Omega 3 (8), 10042–10047. https://doi.org/10.1021/acsomega.8b01626.

Hoke, E.T., Slotcavage, D.J., Dohner, E.R., Bowring, A.R., Karunadasa, H.I., McGehee, M. D., 2015. Reversible photo-induced trap formation in mixed-halide hybrid perovskites for photovoltaics. Chem. Sci. 6 (1), 613–617. https://doi.org/10.1039/C4SC03141E.

Kato, Y., Ono, L.K., Lee, M.V., Wang, S., Raga, S.R., Qi, Y., 2015. Silver iodide formation in methyl ammonium lead iodide perovskite solar cells with silver top electrodes. Adv. Mater. Interf. 2 (13), 1500195. https://doi.org/10.1002/admi.201500195.

Boyd, C.C., Cheacharoen, R., Leijtens, T., McGehee, M.D., 2019. Understanding degradation mechanisms and improving stability of perovskite photovoltaics. Chem. Rev. 119 (5), 3418–3451. https://doi.org/10.1021/acs.chemrev.8b00336.

Li, M., Zuo, W.-W., Wang, Q., Wang, K.-L., Zhuo, M.-P., Köbler, H., Halbig, C.E., Eigler, S., Yang, Y.-G., Gao, X.-Y., Wang, Z.-K., Li, Y., Abate, A., 2020a. Ultrathin nanosheets of oxo-functionalized graphene inhibit the ion migration in perovskite solar cells. Adv. Energy Mater. 10 (4), 1902653. https://doi.org/10.1002/aenm.201902653.

Huang, Z., Hu, X., Liu, C., Meng, X., Huang, Z., Yang, J., Duan, X., Long, J., Zhao, Z., Tan, L., Song, Y., Chen, Y., 2019. Water-resistant and flexible perovskite solar cells via a glued interfacial layer. Adv. Funct. Mater. 29 (37), 1902629. https://doi.org/10.1002/adfm.201902629.

Li, Z., Liu, N., Liu, Z., Wang, X., Hu, Y., Xu, Q., Li, S., Qiao, Z., Cheng, L., Wang, C., Meng, K., Chen, G., 2020b. A cross-linked PCBM interlayer for efficient and UV-stable methylammonium-free poerovskite solar cells. Energy Technol. 8 (7), 2000224. https://doi.org/10.1002/ente.202000224.

Kim, W., Park, J.B., Kim, H., Kim, K., Park, J., Cho, S., Lee, H., Pak, Y., Jung, G.Y., 2019. Enhanced long-term stability of perovskite solar cells by passivating grain boundary with polydimethylsiloxane (PDMS). J. Mater. Chem. A 7 (36), 20832–20839. https://doi.org/10.1039/C9TA06688H.

Ye, X., Cai, D., Ruan, X., Cai, A., 2018. Research on the selective adhesion characteristics of polydimethylsiloxane layer. AIP Adv. 8 (9), 95004. https://doi.org/10.1063/1.5041867.

Mabrouk, S., Bahrami, B., Gurung, A., Reza, K.M., Adhikari, N., Dubey, A., Pathak, R., Yang, S., Qiao, Q., 2017. Higher efficiency perovskite solar cells using additives of LiI, LiTFSI and BMImI in the PbI2 precursor. Sustain. Energy Fuels 1 (10), 2162–2171. https://doi.org/10.1039/C7SE00435D.